COBEM 2023 27TH INTERNATIONAL CONGRESS OF MECHANICAL ENGINEERING

ABCM Brazilian Society of Mechanical Sciences and Engineering
27th ABCM International Congress of Mechanical Engineering
December 04-08, 2023, Florianópolis-SC, Brazil

COB-2023-1350
MECHANICAL PERFORMANCE OF INCONEL 625 PROCESSED BY L-DED ADDITIVE MANUFACTURING

Juliane Ribeiro da Cruz
Henrique Santos Ferreira
Anselmo Thiesen Júnior
Senai Innovation Institute for Manufacturing Systems and Laser, Arno Waldemar Döhler, 308, Santo Antônio, Joinville, SC - 89218153, Brazil.
juliane.alves@sc.senai.br
henrique.santos@sc.senai.br
anselmo.thiesen@sc.senai.br

Jurandir Marcos Sá de Sousa
Senai Innovation Institute for Manufacturing Systems and Laser, Arno Waldemar Döhler, 308, Santo Antônio, Joinville, SC - 89218153, Brazil.
Precision Engineering Laboratory, Federal University of Santa Catarina, Campus Reitor João David Ferreira Lima, s/n°, Trindade, Florianópolis, SC - 88040900, Brazil.
jurandirmarcos37@gmail.com

Abstract. *Additive manufacturing of Inconel 625 as an alternative to conventional methods is of interest due to its low machinability. This work investigates the mechanical properties of Inconel 625 specimens processed by laser direct energy deposition (L-DED) in the as-built and heat-treated conditions (900 °C for 2 h). Microstructure was characterized by optical and scanning electron microscopy with energy dispersive spectroscopy. Mechanical properties were assessed by Vickers hardness measurements, tensile, and Charpy impact test. The effects of building orientation and heat-treatment are discussed, and results are benchmarked to those of wrought Inconel 625 reported in literature. As-built samples developed a columnar dendritic microstructure with the presence of Mo and Nb-rich interdendritic Laves phase. Heat treatment led to partial recrystallization and segregation of laves phase to grain boundaries, which caused a Charpy energy absorption reduction of about 40%, in comparison to the as-built condition, that was similar to the wrought Inconel 625. Under tensile solicitations, the grain boundary embrittlement reduced the total elongation but did not compromise yield strength and ultimate tensile strength, that remained superior to those of the reference Inconel 625. Slightly superior hardness, yield strength and ultimate tensile strength were found for horizontal specimens, associated with higher cooling rates.*

Keywords: *Inconel 625, L-DED processing, heat-treatment homogenization, refined structure, embrittlement mechanism.*

1. INTRODUCTION

Inconel 625 is a nickel Ni-based superalloy with face-centered cubic structure, whose strengthening originates from solid-solution hardening promoted by the additions of chromium, molybdenum, niobium, and carbon, as well as by precipitation hardening induced by the formation of intermetallics and carbides. In this material, intermetallic are most commonly referred to as Laves phase, which consist of Ni_2(Mo, Nb) compounds with hexagonal crystal structure, dispersed within the Ni-rich matrix (Volpato et al., 2022)

The presence of the Laves phase in Ni-based superalloys, such as Inconel 625 and Inconel 718, can have a significant impact on the mechanical properties because of the compromise between precipitation hardening by Laves phase formation and the decrease in solid-solution strengthening by depletion of Mo and Nb. Additionally, Laves phase is hard and brittle, establishing sites for the nucleation and propagation of cracks (Sui et al., 2017; Volpato et al., 2022), turning the manufacturing of Inconel 625 parts into a complex task due to its high abrasiveness, poor machinability and low thermal conductivity (Dubiel and Sieniawski, 2019). Nevertheless, Inconel 625 is currently used in critical components (e.g., turbine blades, reactors, valves, and heat-exchangers) of high-tech industrial sectors (e.g., aeronautic, aerospace, marine, and petrochemical) due to a set of properties that combine high corrosion and oxidation resistance with superior ductility, tensile strength and impact toughness (Barragan et al., 2021; Kumar et al., 2021).

To overcome these difficulties, processing of these alloys by additive manufacturing (AM) has been used as an alternative (Sui et al., 2017; Dubiel and Sieniawski, 2019; Dutkiewicz et al., 2020; Danielewski and Antoszewski, 2020; Verdi et al., 2021; Kumar et al., 2021). Among the AM techniques, laser directed energy deposition (L-DED) stands out due to relatively high deposition rates, in comparison to other popular techniques such as L-PBF. In this process, a

feedstock material is provided simultaneously with a laser energy source, which melts it and deposits it to a substrate (ASTM F3187, 2016). Numerous feedstocks, whether in the state of wire or metal powder can be processed by L-DED. Besides the ability to process complicated materials, the L-DED technique also differs from other conventional techniques by allowing the building of near net-shape customized geometries, decreasing the post-finishing labor. Besides, other advantages such as the obtention of refined microstructures, low level of distortions, and accurate heat input control are also expected. In this sense, new and worn-out Ni-based alloy components have been manufactured and/or repaired by means of L-DED processing (Dubiel and Sieniawski, 2019).

Despite the above mentioned advantages, L-DED process involves complex interactions that include multiple fast heating and cooling cycles that change based on the processing conditions and materials (Barragan et al., 2021). Elevated thermal gradients and solidification ratios can generate residual stresses, defects (e.g., cracks and delaminations), chemical composition modification, formation of uneven microstructure and, therefore, a decrease in mechanical resistance. Anisotropic behavior perceived in L-DED as-built parts is known to occur by fast cooling, formation of metastable constituents, segregation of phases at grain boundaries, and several different grain growth directions (Dass and Moridi, 2019; Nguejio et al., 2019). Due to the anisotropic inherent nature of Inconel 625 processed by L-DED, post heat-treatment is usually required to reduce residual stresses, homogenize the microstructure, and improve mechanical properties (Hu et al., 2018; Nguejio et al., 2019; Wang et al., 2021; Verdi et al., 2021; Volpato et al., 2022; Wang et al., 2022; Tudu et al., 2023).

This work investigates the microstructure and the tensile and impact properties of Inconel 625 parts processed by additive manufacturing using the laser direct energy deposition (L-DED) process, in the as-built and heat-treated conditions, assessing the effects of building orientation in relation to the substrate (vertical or horizontal). Results are benchmarked to those of commercial Inconel 625 reported in literature. This work provides insights on how the metallurgical changes caused by heat-treatment and build orientation affect the microstructure and properties of this material, contributing to optimize the engineering of Inconel 625 (and similar alloys) additively manufactured parts.

2. MATERIALS AND METHODS

As-received wrought AISI 316 stainless steel (250×250×50 mm) was used as the substrate. Before deposition, substrates were sandblasted and cleaned in ethyl alcohol. Gas-atomized Inconel 625 Ni-based alloy 53-150 µm powder (Höganäs S/A) was employed as feedstock. Pre-tests to check the powder feed rate were performed using a glass beaker and a MARTE AD3300 precision scale (0.01 g). Table 1 shows the chemical composition of the substrate and feedstock as supplied by the manufacturers.

Table 1. Chemical composition of the 316 stainless steel substrate, and Inconel 625 Ni-based alloy feedstock as supplied by the manufacturers.

Elements, wt.%	Cr	Mn	Mo	Si	C	P	Fe	Ni
316 Substrate	17.8	1.2	0.2	0.5	0.04	0.02	Bal.	8.0
Inconel 625 Feedstock	22.0	0.45	9.2	0.5	0.02	0.45	1.0	Bal.

The L-DED system used was the RPMI 535® model, from RPM Innovations Inc. Processing was carried out under an inert argon gas atmosphere, where the oxygen-content was kept below 10 ppm. The machine was coupled to a continuous Ø100 µm fiber laser source doped with Ytterbium (Yb) with a maximum rated laser power of 3300 W (YLS-3000-CT) and 1064 nm ʎ from IPG Photonics® manufacturer. The Beam Parameter Product (BPP = 10.0), and the Beam Quality Parameter (M^2 = 29.7) were measured using the Focus Monitor FM+ beam profilometer from PRIMES GmbH. A 25° discontinuous 4-coaxial nozzle was used in this work.

In a prior design of experiments (DoE) with steps of single beads, single layers, and multilayer geometries, L-DED parameters employed in this work were optimized. Details of the method used for processing parameters optimization can be found elsewhere (Thiesen Jr., 2021; Gutjahr, 2023). Two building sets were manufactured using the optimized parameters, for studies in the as-built and heat-treated conditions. Each building set included cubic samples for microstructure and density characterization, cylindrical and rectangular samples for the tensile test in the vertical and horizontal direction, respectively, and rectangular samples for the Charpy V-notch impact test in the vertical and horizontal orientations. For manufacturing, a slicing strategy of 45° rotation angle between layers was used. Table 2 shows the L-DED parameters used as well as the sample as-built dimensions.

Table 2. L-DED processing parameters and the as built dimensions of additively manufactured samples.

L-DED parameters	Value	Set of Test Samples	Dimensions, mm	Quantity
Spot size, mm	1.78	Tensile Horizontal	80 × 20	8
Powder Feedrate, g/min	15	Tensile Vertical	Ø16 × 80	8
Laser Power, W	550	Impact Charpy Horizontal	60 × 12	10
Travel Speed, mm/min	457	Impact Charpy Vertical	12 × 60	10
Hatch Spacing, mm	1	Cubes	25 × 25 ×25	2
Layer height, mm	0.64	-	-	-

After being manufactured, samples were separated from the 316L substrate by wire-EDM cutting. Half of the samples were submitted to annealing at 900 °C for 2h followed by furnace cooling. Similar heat-treatment conditions were used by Verdi et al. (2022), that reported the obtention of highly competitive mechanical properties. Heat-treatments in the temperature and time range of 700-1200 °C and 1-2 hours have also been attempted by other researchers (Hu et al. 2018; Kumar et al., 2021; Volpato et al., 2022). Afterwards, tensile and V-notched Charpy specimens were machined to meet the standard dimensions reported in ASTM E8/E8M (2022) and ASTM E23 (2018), respectively. Figure 1 illustrates the aspect of the builds, heat-treatment route, and the aspect of the machined samples.

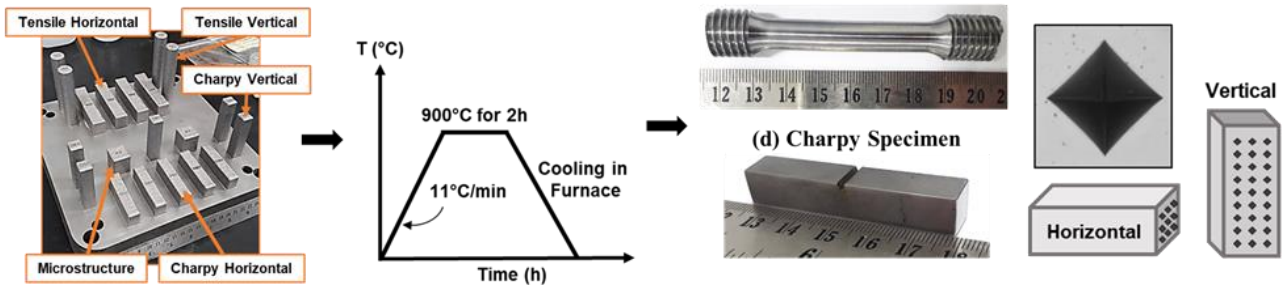

Figure 1. (a) Aspect of the build showing samples additively manufactured by L-DED, (b) Annealing heat-treatment route, aspect of (c) tensile and (d) Charpy specimens and (e) location of Vickers hardness indentations in specimens built in the vertical and horizontal orientations versus the substrate.

For density measurement, cubes were weighed in an Archimedes scale METTLER ME204/A. For microstructure characterization, cubes in the as-built condition and after heat-treatment were subjected to a standard metallographic preparation by cross-sectioning, hot mounting, grinding (#80-1200 Mesh) and polishing down to 0.3 µm diamond suspension. Chemical etching was performed by immersion of the previously warmed samples in fresh Aqua Regia solution. As-built and annealed samples were analyzed by optical microscopy (OM, ZEISS AXIO M2M), scanning electron microscopy and electron dispersive x-ray spectroscopy (SEM and EDS, PHENOM^{TM} proX).

The characterization of mechanical properties was performed by means of hardness (WILSON 402 MVD tester), tensile (INSTRON 5988 universal tester) and Charpy impact tests (INSTRON SI-1D3 tester). Samples in both vertical and horizontal orientations, and in the as-built and solution annealed conditions, were tested, accounting for a total of four different set of samples. The Vickers hardness was calculated as the average of at least 27 indentations taken under a load of 500g (HV0.5) over three profiles on cross-section samples drawn from the cubes (vertical) and from Charpy impact samples built in horizontal orientation (horizontal), as shown in Figure 2. Results obtained were compared with values found in the literature for the commercial Inconel 625 substrate. At least 4 tensile and 5 Charpy impact specimens were tested for each condition. After testing, the macroscopic aspects of tensile and Charpy fracture samples were evaluated using an optical stereoscope (OS, ZEISS DISCOVERY V8) and the microscopic aspect using SEM. Figure 1d illustrates the location of Vickers hardness measurements.

3. RESULTS AND DISCUSSION

The microstructure, hardness, and mechanical properties (tensile and impact) results are presented in this section, highlighting the macro and microscopic features, and the effect of heat-treatment and building orientation. Results are compared and discussed in light of previous work reported in literature.

3.1 Macroscopic features

The macroscopic aspect of samples in the as-built and heat-treated conditions is seen in Figure 2, which shows that the selected L-DED parameters resulted in a microstructure with a high degree of densification and structural integrity, without major defects such as cracks or a lack of fusion. This indicates that the selected L-DED parameters had sufficient

energy to promote metallurgical bond between single beads and single layers. Some degree of round-shaped micro porosities were detected, mostly within the molten pool boundaries, which is characteristic of the gas blisters entrapment during AM L-DED processing (Fiorentin et al., 2022, Paes et al., 2022). Still, an Archimedes density of 8.50 g/cm^3 was achieved, which corresponds to a 98.9% bulk densification (8.6 g/cm^3 was used as a reference). Samples showed no appreciable variations from the three-dimensional CAD model, indicating that the Z-axis increment was not significantly affected by distortions or excessive standoff displacement characteristic of excessive heat input (Yu et al., 2018).

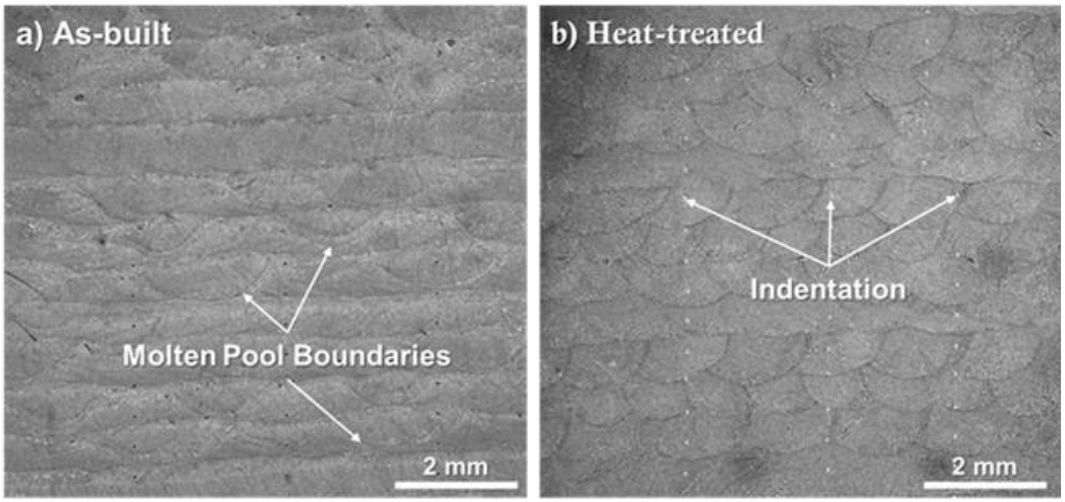

Figure 2. Optical stereoscope images of samples in the a) as-built and b) heat-treated condition showing the macroscopic aspect of samples and the bead deposition structure.

3.2 Effect of heat-treatment on microstructure

Figure 3 shows optical microscopy images of the as-built and heat-treated conditions. In the as-built state (Figure 3a), a full columnar dendritic structure was observed. This structure is known to occur in molten pools, where different grain growth orientations evolve as result of epitaxial growth from numerous nucleation sites at grain boundaries. Besides, dendritic solidification is also very characteristic of processes where fast heating/cooling/solidification cycles occur, such as in AM L-DED, and has been observed by other authors (Marchese et al., 2017; Danielewski and Antoszewski, 2020; Barragan et al., 2021; Verdi et al., 2021; Wang et al., 2022; Tudu et al., 2023;).

On the other hand, a different microstructure was found in samples in the heat-treated state, where the columnar grains underwent a partial transformation into equiaxed grains. Dendritic arms, columnar grains, and heterogeneity in the grain growth directions could still be seen in some areas. In this case, it is reasonable to assume that only a partial recrystallization occurred, as the annealing parameters were not sufficient to fully erase the sample's thermal history. Similarly to what was seen in Figure 2, just a few rounded shape porosities were found here, along with no other defects. Similar effects have been reported in the literature (Reddy et al., 2018; Dubiel and Sieniawski, 2019; Wang et al., 2022).

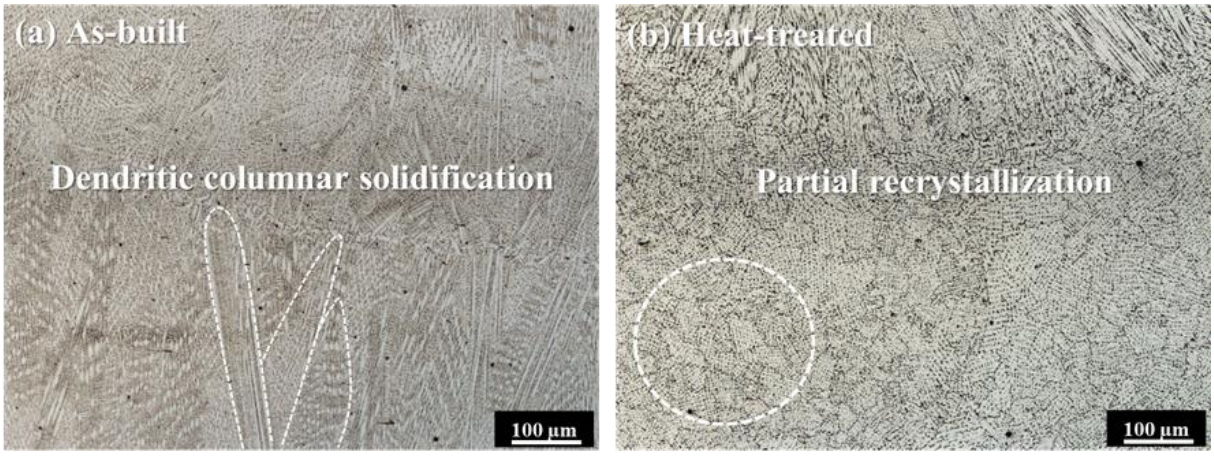

Figure 3. Optical microscopy of Inconel 625 samples built by L-DED a) before and b) after heat-treatment showing columnar dendritic grains in the a) as-built and partial recrystallization in the b) heat-treated condition.

Scanning electron microscopy was used to investigate the microstructure of both as-built and heat-treated samples under higher magnifications and results are shown in Figure 4, in which significant contrast is seen between the as-built fully columnar dendritic structure and the heat-treated recrystallized one. In the as-built condition, primary and secondary dendritic arms with different growth orientations are seen (Figure 4a). With heat-treatment, such refined dendritic structure is replaced by coarser recrystallized grains (Figure 4b). Under high magnification, Laves phase precipitates were seen in the interdendritic region of the as-built samples (Figure 4c) and at the grain boundaries of the sample in the heat-treated condition (Figure 4d). EDS chemical composition by point ID analysis in the matrix and precipitates of Figure 4d is shown in Table 3, and confirm that the precipitates consist of Nb and Mo-rich phase, as expected of Laves phase. Due to a higher degree of vacancies and activity, grain boundaries are usually a preferential site for precipitation. Nguejio et al. (2019) investigated the microstructure of Inconel 625 after annealing at higher temperatures (1100 °C for 1 hour followed by air cooling) and found that heat-treatment promoted interdendritic precipitates solubilization in the austenitic matrix as the grains grew coarser. Although this mechanism could be somewhat occurring in the samples of this study, the larger precipitate sizes found in the heat-treated state, as seen in Figure 4d in comparison to Figure 4c, suggests that laves phase most likely migrated to or grew at the grain boundaries rather than was solubilized during annealing and re-precipitated during cooling. The microstructure features observed here are in accordance with those reported by other authors in the literature (Nguejio et al., 2019; Verdi et al., 2021; Tudu et al., 2023).

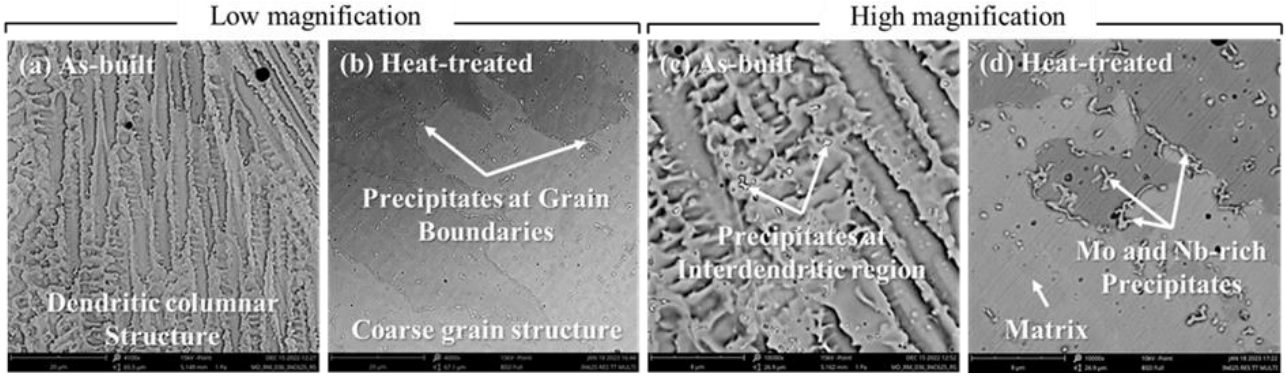

Figure 4. Microstructure of the sample in the (a) as-built and (b) heat-treated condition showing the contrast between the dendritic solidification structure and the recrystallized heat-treated structure. Higher magnification images show the presence of Nb and Mo-rich Laves phase in the (c) interdendritic region and (d) at the grain boundaries of as built and heat-treated samples, respectively.

Table 3. Chemical composition of matrix and precipitates of Figure 4d as measured by EDS point ID analysis in three different locations, showing that precipitates have higher content of Mo and Nb.

Elements, wt%	Ni	Cr	Mo	Nb	Fe+Si+Mn
Ni-matrix	62.6±1.9	17.5±1.8	13.1±1.6	3.3±0.4	<3.6
Interdendritic Precipitates	53.3±2.3	17.4±0.4	16.8±0.5	8.5±1.4	<4.0

3.3 Effect of build orientation on microstructure and hardness

Figure 5 shows the impact of building orientation on the macroscopic aspect and hardness of the Inconel 625 samples manufactured by AM L-DED. In the as-built condition, the sample manufactured in the horizontal orientation (Figure 5a) developed a higher hardness and slightly smaller beads in comparison with the sample built in the vertical orientation (Figure 5b). This behavior is associated with the higher contact area between substrate and/or previously deposited layer, that allows for a more effective heat conduction from the part being deposited to the substrate and a higher cooling rate. In vertical samples, however, the conduction heat-sink mechanism is less effective, and the cooling rate is smaller because of the reduced contact area between the layers. This kinetics is also influenced by the layer deposition time. For the same AM L-DED parameters, a layer takes longer to be deposited in the horizontal orientation in comparison to the vertical one, which gives the first scenario more time for the heat-sink action. Thus, the resulting microstructure is more refined, which is known to increase the hardness (Marchese et al., 2017) This agrees with findings reported by several authors in the literature (Danielewski and Antoszewski, 2020; Barragan et al., 2021; Fiorentin et al., 2022).

After the annealing heat-treatment, the hardness of samples deposited in the horizontal (Figure 5c) and vertical orientations (Figure 5d) was significantly reduced. This is due to the recrystallization phenomenon previously shown in Figure 3b and Figure 4b. Recrystallization coarsened the grain size and enhanced the concentration of Laves phases at grain boundaries. This is known to deplete the Ni-matrix of high-strength solid-solution hardening elements, such as Mo and Nb, accounting for a drop in hardness (Marchese et al., 2017; Nguejio et al., 2019; Dutkiewicz et al., 2020).

Box plot graphs of hardness values of all samples are shown in Figure 5e and are compared to that of a commercial Inconel 625 extracted from literature (Ramkumar et al., 2017). ANOVA analysis and Tukey test of mean comparison show that, although a significant hardness difference was seen between the horizontal and vertical samples in the as-built condition, the hardness values measured for heat-treated samples were not significantly different from each other, indicating that some degree of microstructure normalization for these different conditions was achieved. All samples processed by AM L-DED developed a higher hardness in comparison to the commercial Inconel 625 alloy, independently of the building orientation and heat-treatment performed, which is most likely associated with the intrinsically higher cooling rates and refinement of L-DED processed samples.

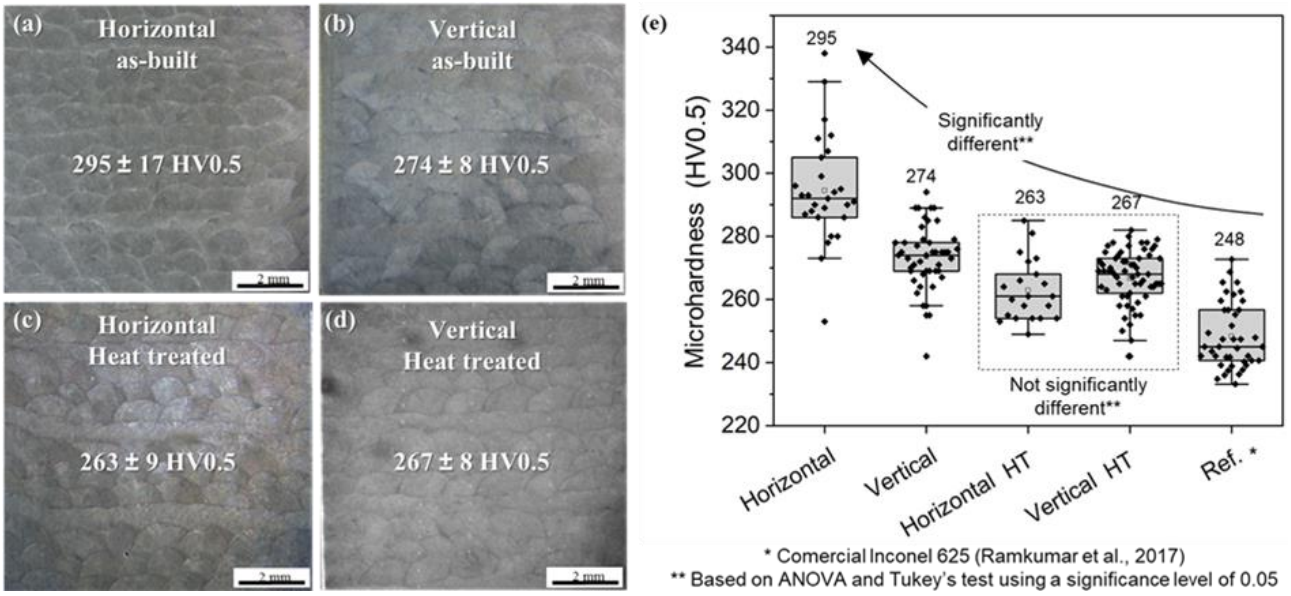

Figure 5. Macroscopic aspect and average hardness (HV0.5) of sample processed in the (a) horizontal orientation, showing a higher hardness and slightly smaller beads than the sample processed in the (b) vertical orientation, due to a higher cooling rate. After heat-treatment, the hardness of samples processed in the (c) horizontal and (d) vertical orientation was significantly reduced, suggesting that the microstructure was somewhat normalized. L-DED samples were found to be harder than the reference material (Ref). *Commercial Inconel 625 (Ramkumar et al., 2017).

3.4 Effect of heat-treatment and build orientation on mechanical properties

Charpy impact test results and fractography are shown in Figure 6. Results were mainly affected by the heat-treatment. Both horizontal and vertical orientations show values around 70 J in the as-built condition, which is consistent with the reference commercial Inconel 625. However, heat-treated samples showed much lower mean absorbed energy (approximately 45 J), in comparison to the as-built specimens and reference material (Ramkumar et al., 2017). Although no significant variations were found as a function of building orientation, it could be expected that the vertical orientation would absorb more energy on impact than the horizontal one, due to a high ductility, as reported by Verdi et al. (2021). The low impact toughness of heat-treated specimens is also related to the microstructure characteristics. Although it was possible to see a combination of brittle fracture cleavage bands and ductile fracture dimples in all of the specimens, clear differences can be observed between the specimens in the as-built and heat-treated conditions as shown in Figure 6b and Figure 6c. While specimens in the as-built condition showed a more ductile mode of failure (Figure 6b), heat-treated specimens showed clear indications of intergranular fracture, characteristic of grain boundary embrittlement (Figure 6c). This is consistent with the segregation of Laves phase to grain boundaries, as seen in Figure 4b and discussed in the previous section, which provides an ideal condition for the nucleation and propagation of cracks (Verdi et al., 2021).

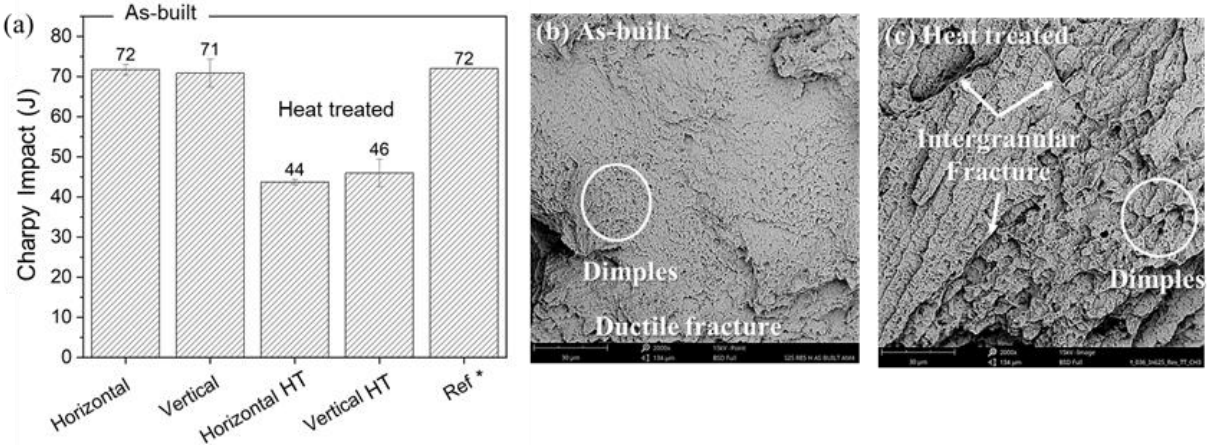

Figure 6. (a) Charpy impact results showing reduced impact toughness of heat-treated specimens, whose grain boundaries were embrittled by Laves phase segregation. Fractography of specimens built in the horizontal orientation illustrate the (b) ductile fracture mode of as built specimens in contrast with the (c) intergranular fracture mode of heat-treated specimens. *Commercial Inconel 625 (Ramkumar et al., 2017).

Tensile stress-strain curves representative of each condition are shown in Figure 7a. It is possible to see that specimens in the as built condition reached higher values of elongation until fracture than the heat-treated specimens, whose grain boundaries were embrittled by segregation of Laves phase, as seen in Figure 6. Unlike the impact test, orientation did have a significant impact in the tensile performance. In Figure 7 it is possible to see that the horizontal specimens showed a trend to have less elongation until fracture and higher resistance than the specimens built in the vertical direction. This is related to the faster cooling and more refined microstructure of specimens manufactured in the horizontal orientation in comparison to the vertical one, whose lower cooling rate and more reheating cycles experienced during manufacturing caused it to be more ductile. Figure 7b shows a nearly linear relation between the yield strength and hardness (Tudu et al., 2023). It was observed that specimens manufactured in the horizontal orientation tended to show higher hardness and yield strength at the expense of lower elongations. All L-DED specimens had higher yield strength than the reference material, commercial Inconel 625 (Ramkumar et al., 2017).

Figure 8 summarizes the elongation and ultimate tensile strength of all conditions in comparison to the reference material. It demonstrates that, even though the heat-treatment reduced elongation due to the segregation of Laves phases at grain boundaries, this had no detrimental effect on the specimen ultimate tensile strength (UTS). It is important to note that the Inconel 625 manufactured by L-DED outperformed the commercial Inconel 625, used as a reference (Ramkumar et al., 2017). There are a variety of descriptions in the literature, particularly when it comes to the effect of solution annealing heat-treatment on mechanical properties (Hu et al., 2018; Wang et al., 2021; Fiorentin et al., 2022). A summary of all mechanical property results is presented in Table 4.

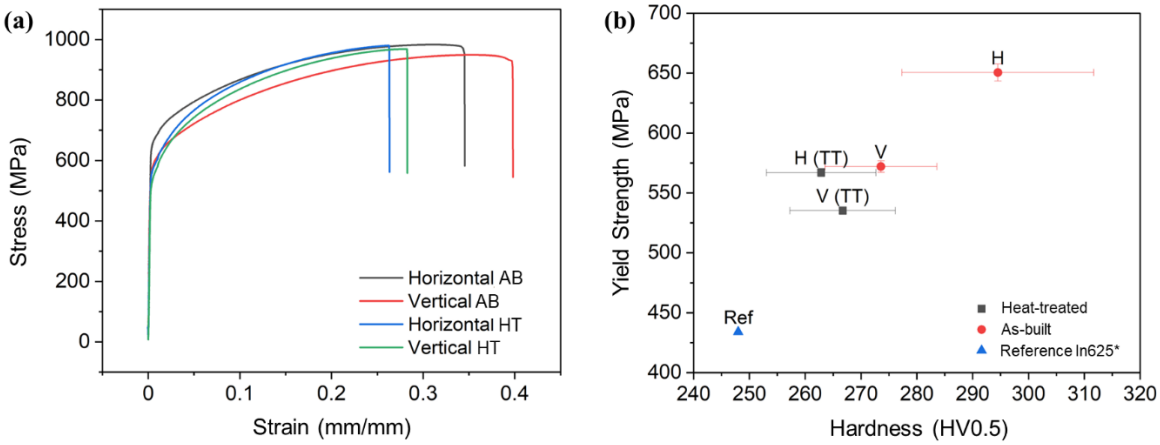

Figure 7. Tensile results: (a) stress-strain curves showing higher ductility of samples in the as-built condition, in comparison to heat-treated ones (with Laves phase segregation at grain boundaries) and of samples manufactured in the vertical orientation, in comparison to those in the horizontal one (with higher hardness associated with higher cooling rates); (b) relation between YS and hardness of AM L-DED samples in comparison to the reference material. Ref: Commercial Inconel 625 (Ramkumar et al., 2017).

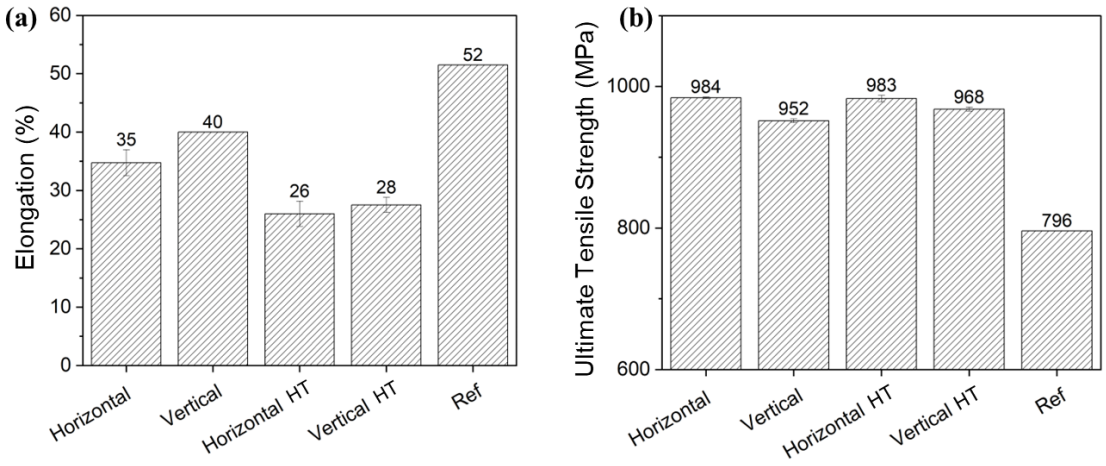

Figure 8. Tensile results: (a) total elongation until fracture, and (b) UTS showing lower elongation until fracture, but much superior UTS of samples manufactured by AM L-DED in comparison to the reference material. Grain boundary segregation induced by heat-treatment affected total elongation but had no significant influence on the UTS. The effect of building orientation was insignificant, but samples built in the horizontal orientation had slightly lower elongation and higher UTS, associated to a higher cooling rate. Ref: Commercial Inconel 625 (Ramkumar et al., 2017).

Figure 9 shows scanning electron microscopy imagens of the tensile test fractures, where it is possible to observe, for all conditions, a large number of dimples along the entire length, revealing the ductile nature for the fracture. This agrees with the elongation, YS and UTS results. Additionally, elongation revealed high values that are comparable to or even higher than those found in the AM L-DED literature, even though it was lowered because of heat-treatment. Despite the absence of cleavage bands and/or any indication of intergranular fracture, the existence of Laves phase does not appear to have had a substantial impact on the fracture development (Dutkiewicz et al., 2020; Wang et al., 2022).

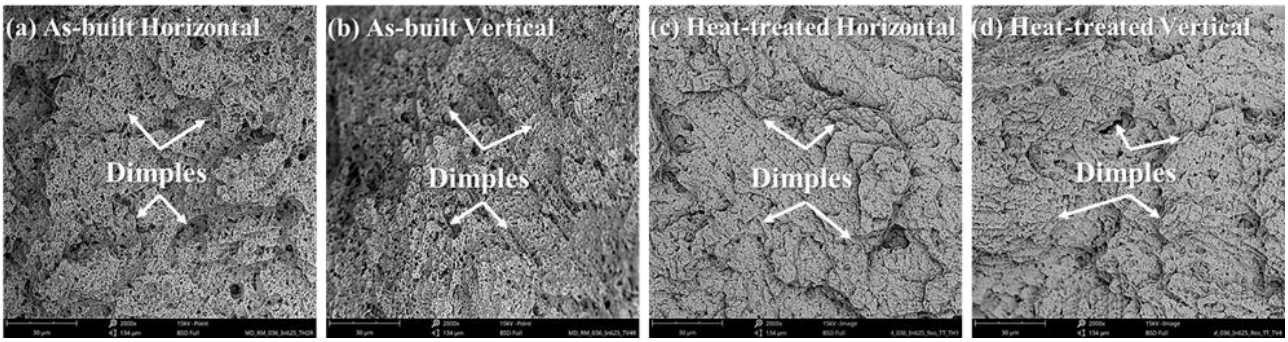

Figure 9. SEM microscopic aspect of tensile fracture samples showing no significant differences among one another: as-built (a) horizontal and (b) vertical; heat-treated (c) horizontal and (d) vertical.

Table 4. Summary of mechanical property results.

In625	UTS, MPa		YS at 0.2%, MPa		Elongation, %		Impact, J		Hardness, HV0.5	
Horizontal AB	984	± 1	650	± 7	35	± 2	72	± 1	294	± 17
Vertical AB	951	± 3	572	± 5	40	± 0	71	± 3	274	± 10
Horizontal HT	983	± 5	567	± 3	26	± 2	44	± 1	263	± 10
Vertical HT	968	± 3	535	± 3	27	± 1	46	± 3	267	± 9
Reference [1]	796		434		51		72		248	

[1] commercial Inconel 625 (Ramkumar et al., 2017)

In summary, results highlight the advantages of the L-DED additive manufacturing of Inconel 625 in terms of mechanical properties and freedom of design with the as-built conditions showing a very competitive performance in comparison to the commercial Inconel 625 alloy. Still, post-processing heat-treatments required because of the complex thermal history of the AM L-DED specimens can lead to the formation of uneven microstructures, and precipitation of undesirable phases that may have a detrimental effect on impact toughness and elongation to fracture. In this regard, it is

essential to properly parameterize the L-DED processing and post-processing heat-treatments to ensure the homogenization of the as-built microstructure, prevent the precipitation of undesirable phases, and reduce the anisotropy phenomenon caused by building orientations to improve mechanical properties, especially regarding elongation and impact resistance.

4. CONCLUSIONS

This work evaluated the microstructure characteristics and mechanical properties of multilayer samples of Inconel 625 additively manufactured by Laser Directed Energy Deposition (AM L-DED). This leads to the following conclusions:

- Processing of Inconel 625 under argon inert environment using L-DED optimized parameters successfully produced multilayer components with a high level of density and no critical defects.
- AM L-DED as-built samples exhibited a refined columnar dendritic microstructure, with Mo and Nb-rich Laves phases at interdendritic regions. After heat-treatment, the microstructure recrystallized and showed coarse grains with a Ni-rich matrix and Laves phase segregation at grain boundaries.
- Hardness, yield strength, elongation, and Charpy impact energy absorption all significantly decreased after heat-treatment of specimen in both orientations associated with grain boundary embrittlement due to Laves phase segregation. The ultimate tensile strength was the only parameter that did not undergo significant changes.
- The specimen processed in the horizontal orientation showed a tendency to have more refined microstructure because of a higher cooling rate. This feature resulted in an increase in hardness, yield strength and ultimate tensile strength, while elongation and Charpy impact energy absorption dropped significantly.
- With the exception of elongation, AM L-DED Inconel 625 specimens displayed compatible and/or superior mechanical responses in terms of hardness, yield strength and ultimate tensile strength in comparison to the commercial Inconel 625.

5. AKNOWLEDGEMENTS

We thank to Senai Innovation Institute for Manufacturing Systems and Laser for their technical-scientific support.

6. REFERENCES

ASTM E23, “Standard Test Methods for Notched Bar Impact Testing of Metallic Materails,”, 2018, *ASTM International*. American Society for Testing and Materials, Pennsylvania, pp. 1-26.

ASTM E8/E8M, “Standard Test Methods for Tension Testing of Metallic Materials,”, 2022, *ASTM International*. American Society for Testing and Materials, Pennsylvania, pp. 1-30.

ASTM F3187, “Standard Guide for Directed Energy Deposition,”, 2016, *ASTM International*. American Society for Testing and Materials, Pennsylvania, pp. 1–22.

Barragan, G., Perilla, D. A. R., Nuñez, J. G., Mariani, F., Coelho, R., 2021, Characterization and Optimization of process parameters for directed energy deposition powder-fed laser system, Journal of Materials Engineering and Performance, v. 30, pp. 5297-5306.

Danielewski, H., Antoszewski, B., 2020, Microstructure and properties of laser additive deposited of nickel base super alloy Inconel 625, v. 2020, pp. 53-59.

Dass, A., Moridi, A., 2019, State of the art in directed energy deposition: from additive manufacturing to materials design, 2019, Coatings, v. 9, pp. 1–26.

Dubiel, B., Sieniawski, J., 2019, Precipitates in additively manufactured Inconel 625 superalloy, Materials, v. 12, pp. 1-11.

Dutkiewicz, J., Rogal, L., Kalita, D., Berent, K., Antoszewski, B., Danielewski, H., Weglowwski, M. S., Lazinska, M., Durejko, T., Czujko, T., 2020, Microstructure and properties of Inconel 625 fabricated using two types of laser metal deposition, Materials, v. 13, pp. 1-17.

Fiorentin, K. F., Maciel, D., Gil, J., Figueiredo, M., Berto, F., Jesus, A., 2022, Fatigue assessment of Inconel 625 produced by directed energy deposition from miniaturized specimens, Metals, v. 12, pp. 1-18. Doi: 10.3390/met12010156.

Gutjahr, J., 2023. *Efeitos da reutilização do pó metálico no processo laser directed energy deposition (L-DED): Uma análise sobre a degradação da matéria-prima e suas consequências no processo e no comportamento de peças fabricadas por manufatura aditiva.* Doctoral thesis, Graduate Program in Mechanical Engineering, Federal University of Santa Catarina, Florianópolis, Brazil.

Hu, Y. L., Lin, X., Zhang, S.Y., Jiang, Y. M., Lu, X. F., Yang H. O., Huang, W. D., 2018, Effect of solution heat treatment on the microstructure and mechanical properties of Inconel 625 superalloy fabricated by laser solid forming, Journal of Alloys and Compounds, v. 767, pp. 330-344.

Kreitcberg, A., Brailovski, V., Turenne, S., 2017, Effect of heat treatment and hot isostatic pressing on the microstructure and mechanical properties of Inconel 625 alloy processed by laser powder bed fusion, Materials Science and Engineering, v. 689, pp. 1-10.

Kumar, S. P., Elangovan, S., Mohanraj, S. E., Ramakrishna, J. R., 2021, A Review on properties of Inconel 625 and Inconel 718 fabricated using direct energy deposition, Materials Today: Proceedings, v. 46, pp. 7892-7906.

Marchese, G., Colera, X. G., Calignaro, F., Lorusso, M., Biamino, S., Minetola, P., Manfredi, D., 2017, Characterization and comparison of Inconel 625 processed by selective laser melting and laser metal deposition, Advanced Engineering Materials, v. 19, pp. 1-9.

Nguejio, J., Szmytka, F., Hallais, S., Tanguy, A., Nardone, S., Martinez, M. G., 2019, Comparison of microstructure features and mechanical properties for additive manufactured and wrought nickel alloys 625, Materials Science and Engineering A, v. 764, pp. 138214.

Paes, L. E.S; Pereira, M.; Xavier, F. A.; Weingaertner, W. L.; Vilarinho, L. O., 2022, Lack of fusion mitigation in directed energy deposition with laser (DED-L) additive manufacturing through laser remelting, Journal of Manufacturing Processes, v. 73, Pp. 67–77.

Ramkumar, K. D., Abraham, W. S., Viyash, V., Arivazhagan, N., Rabel, A. M., 2017, Investigations on the microstructure, tensile strength and high temperature corrosion behaviour of Inconel 625 and Inconel 718 dissimilar joints, Journal of Manufacturing Processes, v. 25, pp. 306–322.

Reddy, L., Preston, S. P., Shipway, P. H., Davis, C., Hussain, T., 2018, Process parameter optimisation of laser clad iron based alloy: Predictive models of deposition efficiency, porosity and dilution, Surface and Coatings Technology, v. 349, pp. 198–207.

Sui, S., Chen, J., Fan, E., Yang, H., Lin, X., Huang, W., 2017, The influence of Laves phases on the high-cycle fatigue behavior of laser additive manufacturing Inconel 718, Materials Science and Engineering A, v. 695, pp. 6-13.

Thiesen Jr, A., 2021. *Selection of processing parameters for the laser directed energy deposition process applied to additive manufacturing: a methodological proposal.* Master's thesis, Graduate Program in Engineering and Mechanical Sciences, Federal University of Santa Catarina, Joinville, Brazil.

Tudu, N., Bruah, M., Prasad, S. B., 2023, Study of laser directed energy deposition of Inconel 625 and austenitic steel, Science and Technology of Welding and Joining, v. 28, pp. 287-297.

Verdi, D., Varadaraju, N., Zhi'En, E. T., Patran, A., 2021, Effect of manufacturing strategy on the toughness behavior of Inconel 625 laser metal deposited parts, Advanced Engineering Materials, v. 23, pp. 2001506.

Volpato, G. M., Tetzlaff, U., Fredel, M. C., 2022, A comprehensive Literature Review on laser powder bed fusion Inconel superalloys, Additive Manufacturing, v. 55, pp. 102871.

Wang, X., Chen, C., Qin, L., Zhang, M., 2021, Microstructure evolution and mechanical behavior of Inconel 625 produced using direct laser metal deposition, Physics of Metals and Metallography, v. 122, pp. 896-907.

Wang, J., Wang, Y., Su, Y., Shi, J., 2022, Evaluation of in-situ alloyed Inconel 625 from elemental powders by laser directed energy deposition, Materials Science and Engineering A, v. 830, pp. 142296.

Yu, T., Sun, J., Qu, W., Zhao, Y., Yang, L., 2018, Influences of z-axis increments and analyses of defects of AISI 316L stainless steel hollow thin-walled cylinder, The International Journal of Advanced Manufacturing Technology, v. 97, pp. 2203-2220.

7. RESPONSIBILITY NOTICE

The authors are the only responsible for the printed material included in this paper.